Supplement of Atmos. Chem. Phys., 21, 183–200, 2021
https://doi.org/10.5194/acp-21-183-2021-supplement

Atmospheric Chemistry and Physics
Open Access
EGU

Supplement of

Investigating three patterns of new particles growing to the size of cloud condensation nuclei in Beijing's urban atmosphere

Liya Ma et al.

Correspondence to: Xiaohong Yao (xhyao@ouc.edu.cn) and Yujiao Zhu (zhuyujiao@sdu.edu.cn)

List of Text:

Text S1 Model evaluation of organic matter and the inorganic species in $PM_{2.5}$.

Text S2 Characteristics of primary particles in number concentration from traffic, industrial and cooking emissions.

Text S3 Temporal variations in different secondary organic aerosols during NPF events.

List of Figures:

Fig. S1 Domains of the CMAQ simulation.

Fig. S2 Temporal results of $N_{50\text{-}200\ nm}$ (*net*) (a), $N_{70\text{-}200\ nm}$ (*net*) (b), contour plots (c) and the height of planetary boundary layer (d) on 25 August 2014.

Fig. S3 Contour plots of Class I (a), Scenario 1 (c), Scenario 2 (e), Scenario 3 (g) and Scenario 4 (i) of Class II NPF events and corresponding wind speeds and wind directions in (b), (d), (f), (h) and (j).

Fig. S4 NPF events occurred on 12 and 13 July 2014 ((a, e) contour plots of the particle number concentration; (b, f) time series of the observed mixing ratios of SO_2 and NO_2+O_3; (c, g) time series of the modeled SOA, NO_3^- and NH_4^+ in $PM_{2.5}$; (d, h) time series of ambient T and RH).

Fig. S5 NPF events occurred on 12 and 15 August 2014 ((a, e) contour plots of the particle number concentration; (b, f) time series of the observed mixing ratios of SO_2 and NO_2+O_3; (c, g) time series of the modeled SOA, NO_3^- and NH_4^+ in $PM_{2.5}$; (d, h) time series of ambient T and RH).

Fig. S6 NPF events occurred on 25 July and 11 June 2014 ((a, e) contour plots of the particle number concentration; (b, f) time series of the observed mixing ratios of SO_2 and NO_2+O_3; (c) time series of the modeled SOA, semi-SOA, NO_3^- and NH_4^+ in $PM_{2.5}$; (d, h) time series of ambient T and RH; (g) time series of the observed OOA, NO_3^- and NH_4^+ in $PM_{1.0}$).

Fig. S7 Time series of daily mean concentrations of simulated and observed SOA/OOA as well as inorganic species including NO_3^-, SO_4^{2-} and NH_4^+.

Fig. S8 Contour plot of particle number concentrations at the roadside site with spikes from traffic emissions.

Fig. S9 Fresh industrial emissions associated with high SO_2 (12:30-15:00) and cooking emissions with increased cooking OA (COA, 18:20-21:00) on 30 June 2014.

Fig. S10 Contour plot of particle number concentrations during NPF event and variations in hydrocarbon-like OA (HOA), cooking OA (COA), less oxidized oxygenated OA (LO-OOA) and more oxidized oxygenated OA (MO-OOA) on 18 June 2014.

List of Table:

Table S1 Model performance of OOA as well as the inorganic species in $PM_{2.5}$ in Beijing

Text S1 Model evaluation of organic matter and the inorganic species in $PM_{2.5}$

The observed concentrations of oxygenated organic aerosols (OOA) as well as the inorganic species (including NO_3^-, SO_4^{2-} and NH_4^+) in $PM_{1.0}$ measured by High-Resolution Time-of-Flight AMS (HR-ToF-AMS) in 10 minutes time-resolution from 3 June to 11 July 2014 (Xu et al., 2017) were used for model evaluation in study domain (Fig. S1). The sampling site located at a Tower branch of the Institute of Atmospheric Physics in Beijing, China (39.98°N, 116.38°E). Three statistical parameters including Normalized Mean Bias (NMB), Normalized Mean Error (NME), and correlation coefficient (R) were used to evaluate the CMAQ model prediction, using the equations as following (US-EPA, 2007):

$$NMB = \frac{\sum_{i=1}^{n}(Sim_i - Obs_i)}{\sum_{i=1}^{n} Obs_i} \times 100\%$$

$$NME = \frac{\sum_{i=1}^{n}|Sim_i - Obs_i|}{\sum_{i=1}^{n} Obs_i} \times 100\%$$

$$R = \frac{\sum_{i=1}^{n}((Sim_i - \overline{Obs}) \times (Obs_i - \overline{Obs}))}{\sqrt{\sum_{i=1}^{n}(Sim_i - \overline{Sim^2}) \times \sum_{i=1}^{n}(Obs_i - \overline{Obs^2})}}$$

in which, Sim_i represents the concentrations simulated by CMAQ, and Obs_i represents the observation concentrations.

The temporal variations of daily mean concentrations of simulated and observed OOA, NO_3^-, SO_4^{2-} and NH_4^+ were shown in Fig. S7. The model simulation well replicated the temporal variations of OOA, NO_3^-, SO_4^{2-} and NH_4^+ concentrations during the study period. The NO_3^-, SO_4^{2-} and NH_4^+ model results generally could meet the benchmark criteria of above three species (US-EPA, 2007), with correlations of higher than 0.61 (Table S1). The concentrations of SO_4^{2-} and NH_4^+ had been slightly overestimated (with NMBs and 12%, 6%), while the concentrations of NO_3^- and OOA were underestimated (with NMBs of -29% and -90%). NMEs of NO_3^-, SO_4^{2-} and NH_4^+ varied from 50% to 72%, which were smaller than 75% of benchmark criteria. The HR-ToF-AMS detected only chemical species in particles less than 1.0 μm, while the accumulation mode of SO_4^{2-} and NH_4^+ can extend to 1-2 μm. (Yao et al., 2003). The HR-ToF-AMS was set closer to an elevated highway as well as a moderate traffic road behind. The observational values may contain a large contribution from on-road vehicle emissions, and subsequently result in an under-prediction of NO_3^- and OOA in modeling against them. NO_3^- concentrations in $PM_{2.5}$ reportedly exhibited a larger spatial heterogeneity than that of SO_4^{2-} in Beijing (Yao et al., 2002). Additionally, underestimation of SOA is the common weakness of model simulation because a fraction of SOA precursors was not involved such as aromatic volatile organic compounds, SOA yields was underestimated and some key formation pathways of SOA may still miss in current air quality models (Appel et al., 2008; Baek et al., 2011; Hallquist et al., 2009; Knote et al., 2014).

Text S2 Characteristics of primary particles in number concentration from traffic, industrial and cooking emissions.

Particle number size distributions (PNSD) associated with on-road traffic emissions are characterized by two peaks, i.e., about 16 nm and 30 nm, and intermittently lasts a few seconds or minutes (Fig. S8). The spikes of particle number concentrations are expected to be observed when on-road vehicles start to accelerate. Frequent traffic congestion may also lead to the accumulation of traffic-derived particles. PNSD associated with fresh industrial emissions can be identified from the largely increased SO_2 and those associated with cooking emissions can be identified from the largely increased cooking organic aerosols (COA) (Fig. S9). The strong emissions of COA usually occur at the fixed time period, i.e., 18:00-20:00. It is clear that the dominant modes of particles from traffic emissions, industrial emissions and cooking emissions occurred at ~20 nm, ~30 nm and ~40 nm, respectively, and the domain mode size were quietly stable in the study period. Their contributions were probably important to the observed PNSD during non-NPF periods. On the roof sampling site, their contributions to the observed particle concentrations during the initial few hours of NPF were generally negligible in presence of wind speeds of 4-6 m s^{-1}, except a few occasional spikes lasting in minutes. Additionally, their influences can also be ignored in studying the growth of newly formed particles when the particles grew over 50 nm.

Text S3 Temporal variations in different secondary organic aerosols during NPF events.

During the NPF event (e.g. Fig. S9), cooking organic aerosols (COA) occasionally influences the new particles signal, and the growth of new particles is consistent mainly with the increase in MO-OOA and LO-OOA. Therefore, we argue that the growth of newly formed particles depends largely on the condensational growth. Again, the data measured by the paralleling particle sizer operating in one second alone can allow us identifying the signals from primary emissions, regional plumes, etc., and removing them in studying new particle formation events.

References

Appel, K.W., Bhave, P.V., Gilliland, A.B., Sarwar, G., Roselle, S.J.: Evaluation of the community multiscale air quality (CMAQ) model version 4.5: Sensitivities impacting model performance; Part II-particulate matter, Atmos. Environ., 42, 6057-6066, doi:10.1016/j.atmosenv.2008.03.036, 2008.

Baek, J., Hu, Y.T., Odman, M.T., Russell, A.G.: Modeling secondary organic aerosol in CMAQ using multigenerational oxidation of semi-volatile organic compounds, J. Geophys. Res., 116, D22204, doi: 10.1029/2011JD015911, 2011.

Hallquist, M., Wenger, J.C., Baltensperger, U., Rudich, Y., Simpson, D., Claeys, M., Dommen, J., Donahue, N.M., George, C., Goldstein, A.H., Hamilton, J.F., Herrmann, H.. Hoffmann, T., Iinuma, Y., Jang, M., Jenkin, M.E., Jimenez, J.L., Kiendler-Scharr, A., Maenhaut, W., McFiggans, G., Mentel, Th. F., Monod, A., Prevot, A.S.H., Seinfeld, J.H., Surratt, J.D., Szmigielski, R., Wildt, J.: The formation, properties and impact of secondary organic aerosol: current and emerging issues, Atmos. Chem. Phys., 9, 5155-5236, http://www.atmos-chem-phys.net/9/5155/2009/, 2009.

Knote, C., Hodzic, A., Jimenez, J.L., Volkamer, R., Orlando, J.J., Baidar, S., Brioude, J., Fast J., Gentner D.R., Goldstein A.H., Hayes P.L., Knighton W.B., Oetjen H., Setyan A., Stark, H., Thalman, R., Tyndall, G., Washenfelder, R., Waxman, E. and Zhang, Q.: Simulation of semi-explicit mechanisms of SOA formation from glyoxal in aerosol in a 3-D model, Atmos. Chem. Phys., 14, 6213-6239, doi:10.5194/acp-14-6213-2014, 2014.

Xu, W.Q., Han, T.T., Du, W., Wang, Q.Q., Chen, C., Zhang, Y.J., Li, J., Fu, P.Q., Wang, Z.F., Worsnop, D.R., Sun, Y.L.: Effects of aqueous-phase and photochemical processing on secondary organic aerosol formation and evolution in Beijing, China, Environ. Sci. Technol., 51, 762-770, doi: 10.1021/acs.est.6b04498, 2017.

US-EPA, Guidance on the Use of Models and Other Analyses for Demonstrating Attainment of Air Quality Goals for Ozone, PM2.5, and Regional Haze, EPA -454/B-407-002, 2007.

Yao, X.H., Chan, C.K., Fang, M., Cadle, S., Chan, T., Mulawa, P., He, K.B., Ye, B.M.: The water-soluble ionic composition of pm2.5 in Shanghai and Beijing, China, Atmos. Environ., 36, 4223-4234, https://doi.org/10.1016/S1352-2310(02)00342-4, 2002.

Yao, X.H., Lau, A.P.S., Fang, M., Chan, C.K., Hu, M.: Size distributions and formation of ionic species in atmospheric particulate pollutants in Beijing, China: 1—inorganic ions, Atmos. Environ., 37, 2991-3000, https://doi.org/10.1016/S1352-2310 (03)00255-3, 2003.

Fig. S1 Domains of the CMAQ simulation

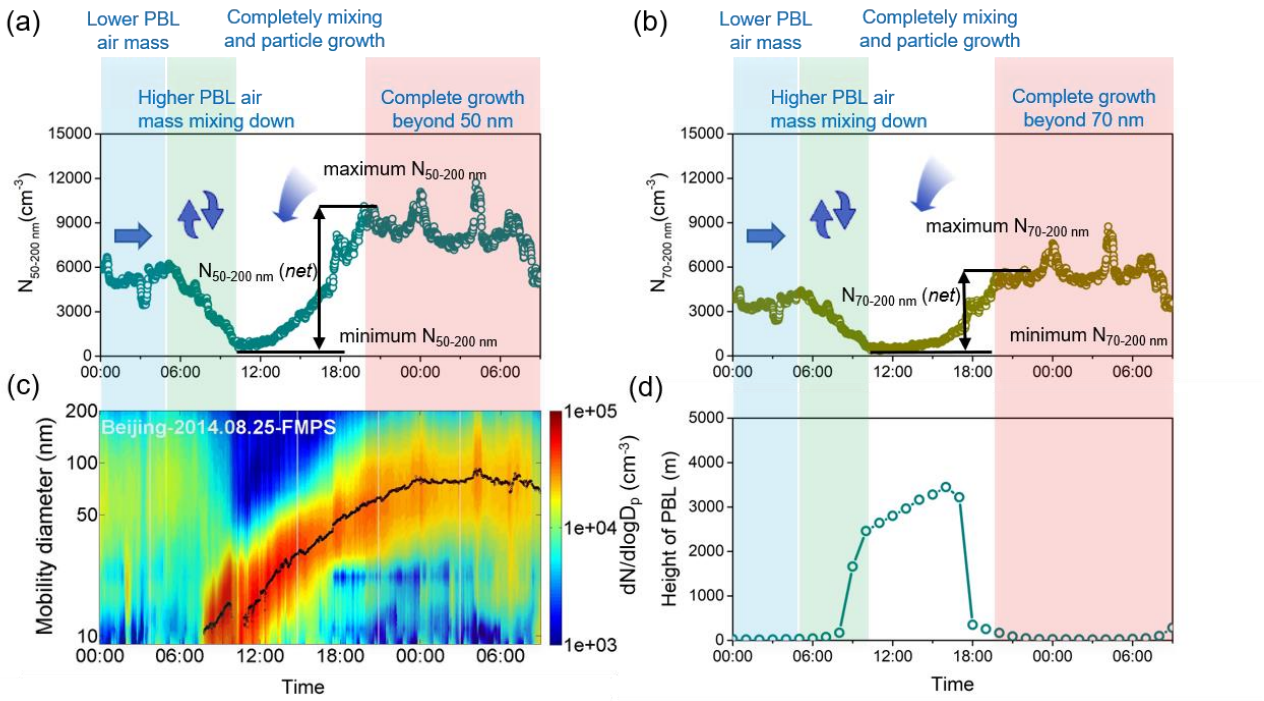

Fig. S2 Temporal results of $N_{50\text{-}200\ nm}$ (*net*) (a), $N_{70\text{-}200\ nm}$ (*net*) (b), contour plots (c) and the height of planetary boundary layer (d) on 25 August 2014. (The height of planetary boundary layer at the nearby site was obtained from the ECMWF reanalysis data, which was downloaded from https://cds.climate.copernicus.eu/cdsapp#!/dataset/reanalysis-era5-single-levels?tab=overview).

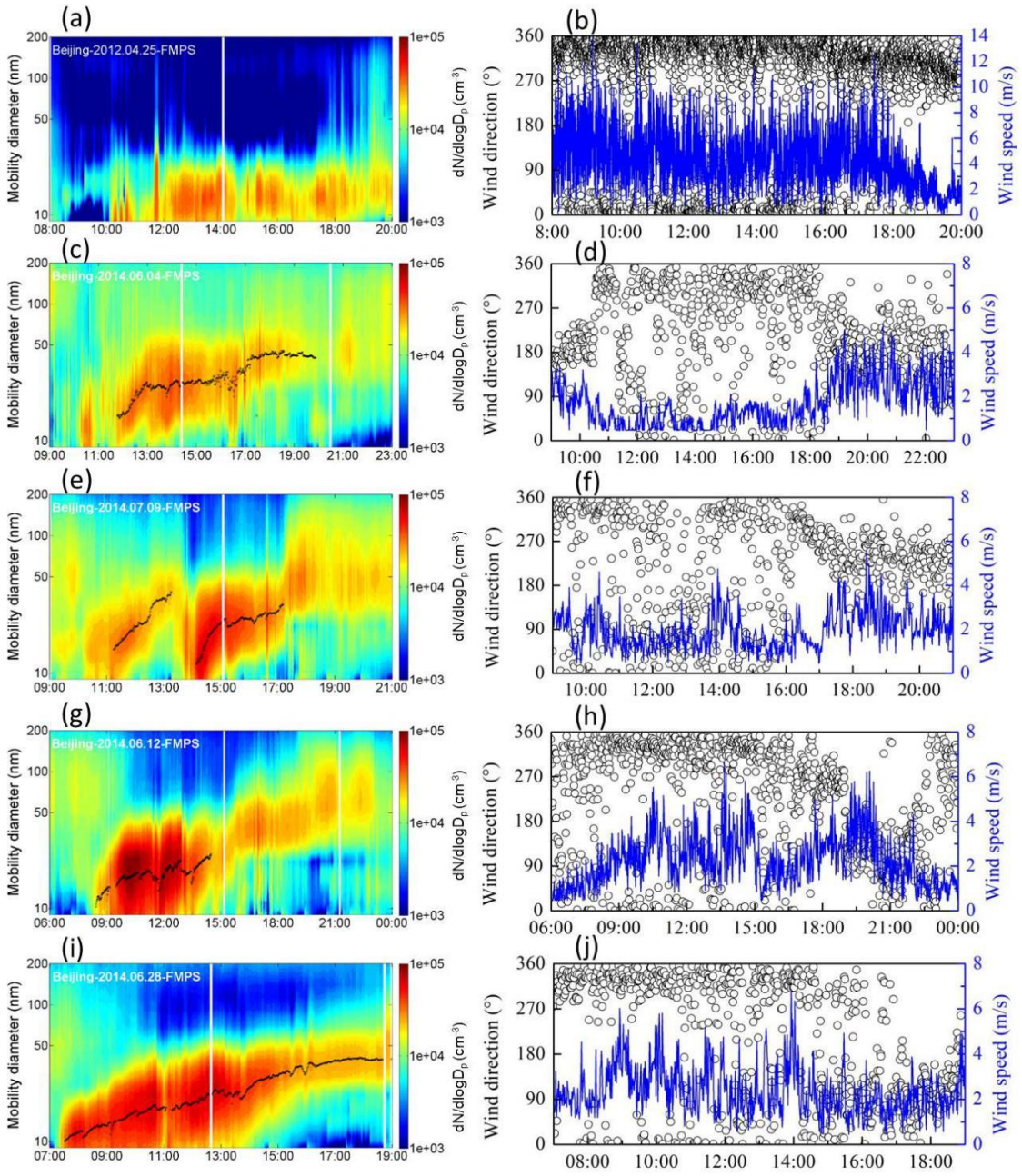

Fig. S3 Contour plots of Class I (a), Scenario 1 (c), Scenario 2 (e), Scenario 3 (g) and Scenario 4 (i) of Class II NPF events and corresponding wind speeds and wind directions in (b), (d), (f), (h) and (j).

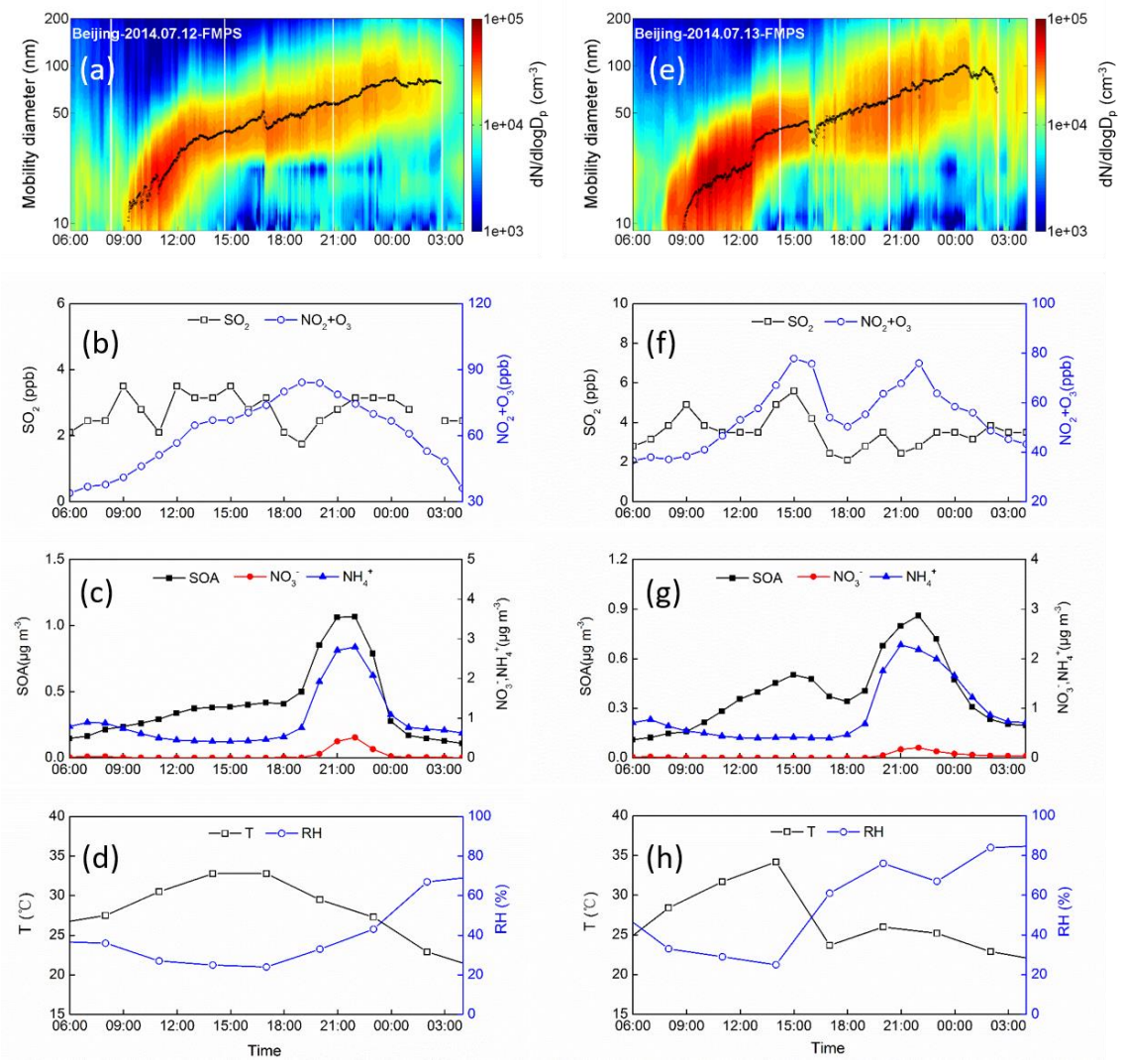

Fig. S4 NPF events occurred on 12 and 13 July 2014 ((a, e) contour plots of the particle number concentration; (b, f) time series of the observed mixing ratios of SO_2 and NO_2+O_3; (c, g) time series of the modeled SOA, NO_3^- and NH_4^+ in $PM_{2.5}$; (d, h) time series of ambient T and RH).

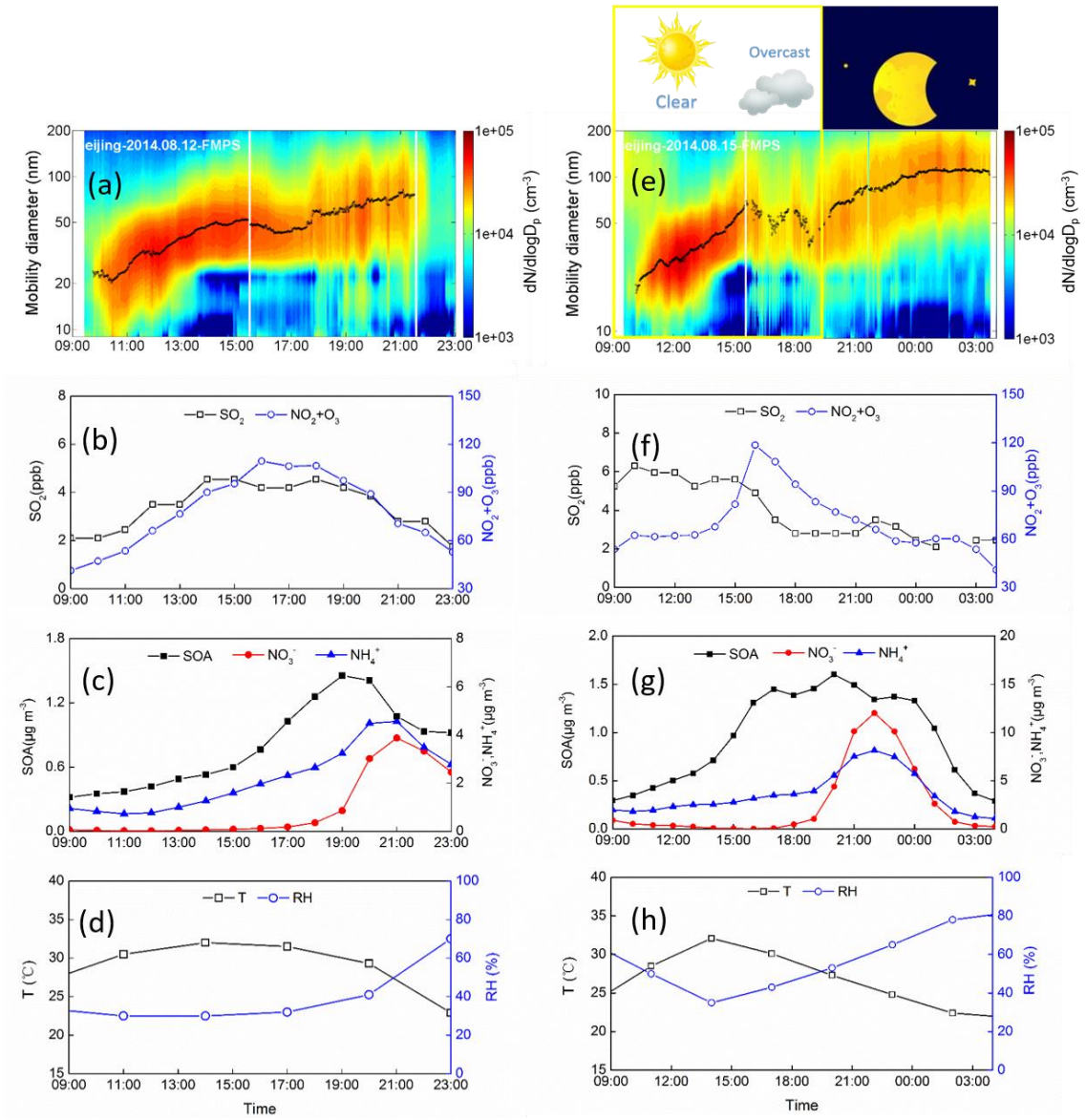

Fig. S5 NPF events occurred on 12 and 15 August 2014 ((a, e) contour plots of the particle number concentration; (b, f) time series of the observed mixing ratios of SO_2 and NO_2+O_3; (c, g) time series of the modeled SOA, NO_3^- and NH_4^+ in $PM_{2.5}$; (d, h) time series of ambient T and RH).

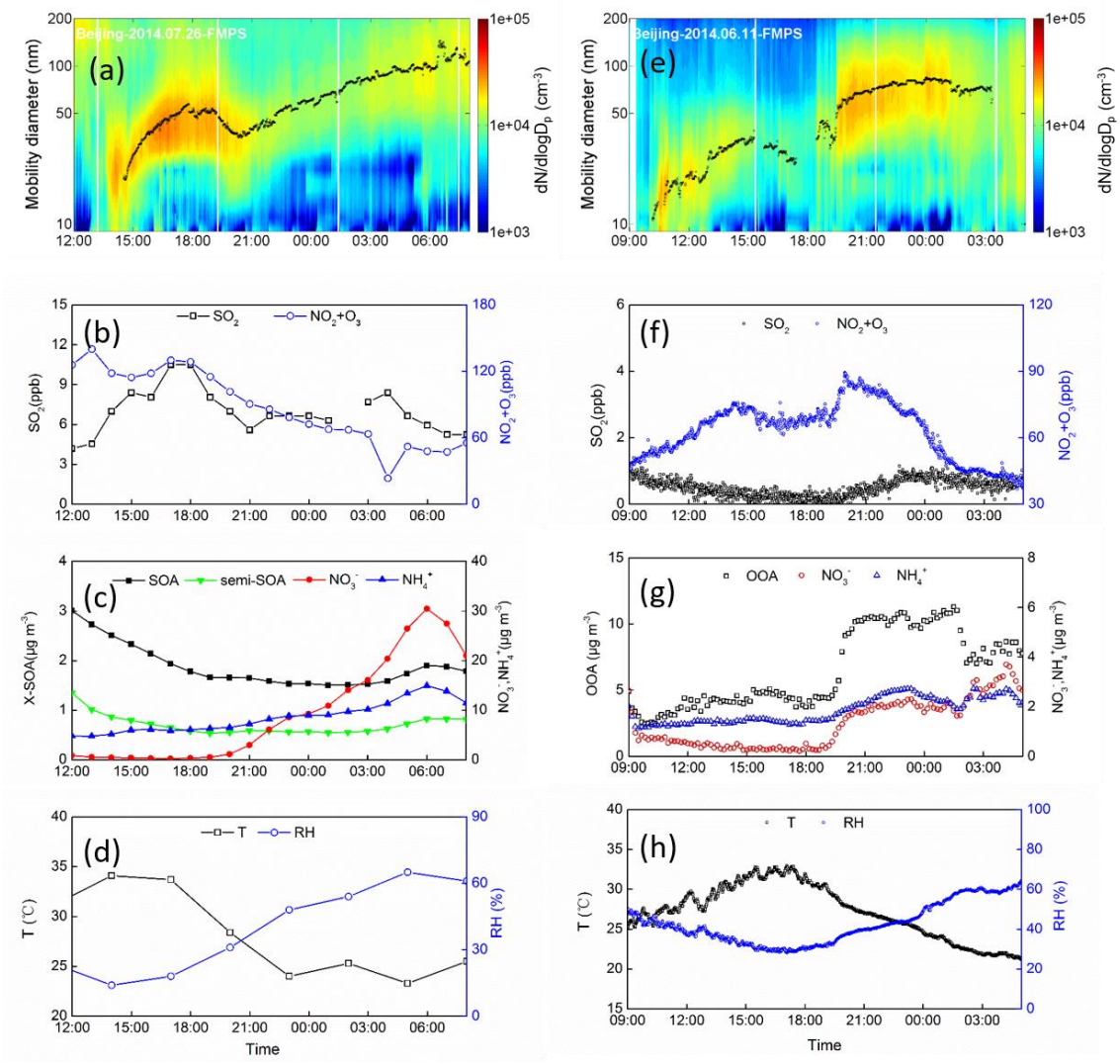

Fig. S6 NPF events occurred on 25 July and 11 June 2014 ((a, e) contour plots of the particle number concentration; (b, f) time series of the observed mixing ratios of SO_2 and NO_2+O_3; (c) time series of the modeled SOA, semi-SOA, NO_3^- and NH_4^+ in $PM_{2.5}$; (d, h) time series of ambient T and RH; (g) time series of the observed OOA, NO_3^- and NH_4^+ in $PM_{1.0}$).

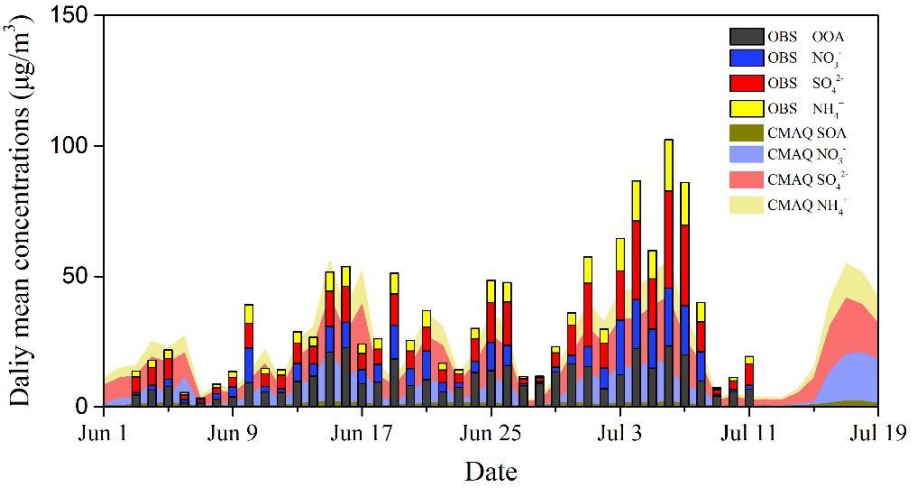

Fig. S7 Time series of daily mean concentrations of simulated and observed SOA/OOA as well as inorganic species including NO_3^-, SO_4^{2-} and NH_4^+.

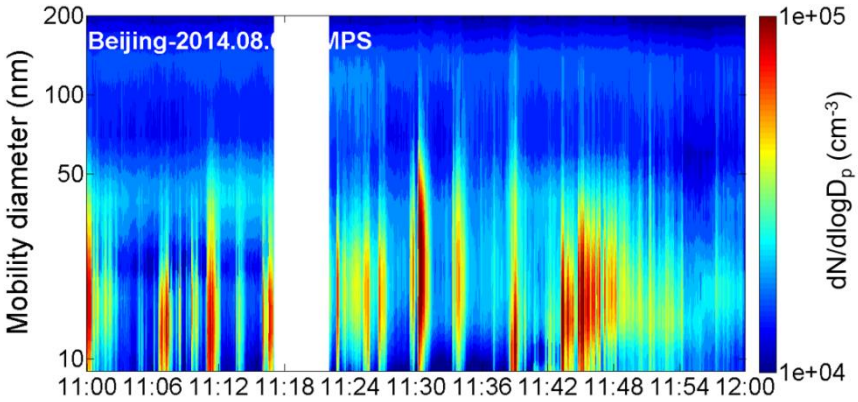

Fig. S8 Contour plot of particle number concentrations at the roadside site with spikes from traffic emissions.

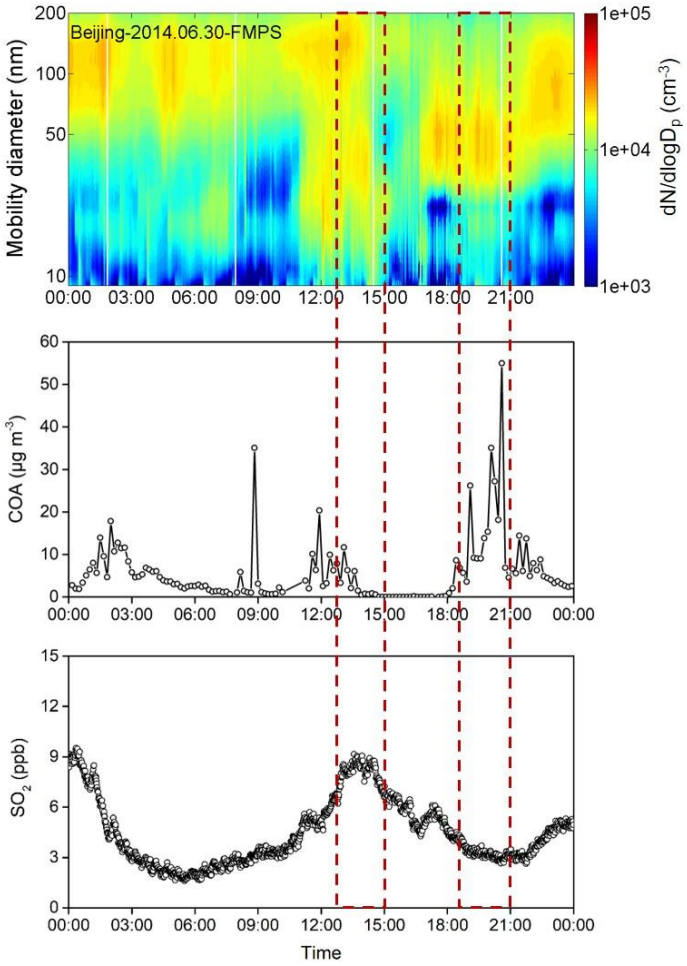

Fig. S9 Fresh industrial emissions associated with high SO_2 (12:30-15:00) and cooking emissions with increased cooking OA (COA, 18:20-21:00) on 30 June 2014.

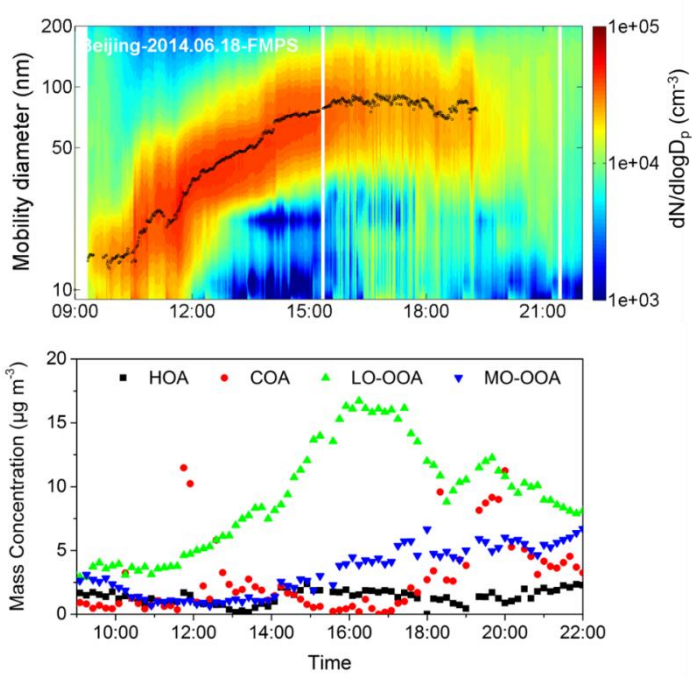

Fig. S10 Contour plot of particle number concentrations during NPF event and variations in hydrocarbon-like OA (HOA), cooking OA (COA), less oxidized oxygenated OA (LO-OOA) and more oxidized oxygenated OA (MO-OOA) on 18 June 2014.

Table S1 Model performance of OOA as well as the inorganic species in $PM_{2.5}$ in Beijing

	OOA	NO_3^-	SO_4^{2-}	NH_4^+
NMB	-90%	-29%	12%	6%
NME	90%	72%	50%	53%
R	0.53	0.61	0.69	0.67